Interdiffusion of CdS/CdTe thin films: Modeling x-ray diffraction line profiles

Brian E. McCandless
Institute of Energy Conversion, University of Delaware, Newark, Delaware 19716

Michael G. Engelmann
TREX Enterprises, 590 Lipoa Parkway, Suite 222, Kihei, Maui, Hawaii 96763

Robert W. Birkmire
Institute of Energy Conversion, University of Delaware, Newark, Delaware 19716

(Received 17 July 2000; accepted for publication 2 October 2000)

A method for analyzing the diffusion process for CdS into CdTe thin films using x-ray diffraction is presented, allowing both bulk and grain boundary diffusion coefficients to be estimated. The equilibrium phase diagram for the $CdTe_{1-x}S_x$ and $CdS_{1-y}Te_y$ alloy system was determined for temperatures from 625 °C to 415 °C. Measured diffraction line profiles for time-progressive diffusion of CdS into CdTe films resulting from thermal treatment at 440° were modeled using bulk and grain boundary diffusion coefficients of 1.25×10^{-13} cm^2/s and 1.5×10^{-8} cm^2/s, respectively. Modeling diffraction line profiles of samples treated at temperatures from 380 °C to 480 °C yielded Arrhenius activation energies for bulk and grain boundary diffusion processes of 2.8 eV and 2.0 eV, respectively. The bulk diffusion coefficients obtained from thin film structures were comparable to those obtained by Auger depth profiles for CdS/CdTe couples using CdTe single crystals. © *2001 American Institute of Physics.* [DOI: 10.1063/1.1330245]

I. INTRODUCTION

Thin film solar cells based on polycrystalline CdTe have demonstrated ~16% solar conversion efficiency[1] but translation of this laboratory result to modules has been difficult. One critical issue is the use of thin, less than 100 nm, CdS films as the heterojunction partner/window layer, which affects the cell/module performance in several ways. Optical absorption in the CdS and $CdS_{1-y}Te_y$ alloys limits light generated current at wavelengths less than below 550 nm. Thus, maximum current generation is obtained for the thinnest CdS films. However, for CdS films less than ~100 nm thick, discontinuities in the CdS layer produce parallel junctions between the CdTe and the transparent conductive oxide, which limits the open circuit voltage.[2] Cell processing promotes intermixing, which reduces the thickness of the CdS layer and is expected to transform the planar as-deposited interface into a three-dimensional structure with respect to S and Te distribution, thereby giving rise to spatial variation in material properties. The principal factors affecting CdS diffusion into CdTe have been empirically identified as CdTe grain size, CdS film growth process, CdS/CdTe postdeposition treatment temperature, and $CdCl_2$:O_2:Ar concentration.[3] Enhanced CdS diffusion has been qualitatively linked to quantitative treatment of the grain boundary diffusion processes[4] and resulting $CdTe_{1-x}S_x$ alloy distribution diffusion dynamics in the thin film couple have relied on the interpretation of averaging depth profile analyses.[5]

In this article, a method for analyzing the diffusion process for CdS into CdTe is presented where specially prepared thin film and single crystal CdTe–CdS samples were analyzed to determine both bulk and grain boundary diffusion coefficients. The method is based on a continuum model of the bulk and grain boundary diffusion and measured grain size distributions and grain boundary widths to generate the $CdTe_{1-x}S_x$ compositional volume fractions needed to synthesize x-ray diffraction (XRD) line profiles. Estimates of both bulk and grain boundary diffusion coefficients were made by regressing measured and predicted XRD line profiles using the diffusion coefficients as the only fitting parameters. To accurately model the $CdTe_{1-x}S_x$ alloy line profiles, the solubility limits of the CdTe–CdS system were established over the temperature range from 420 °C to 625 °C using mixed CdTe–CdS films after prolonged thermal treatment in a $CdCl_2$:O_2:Ar atmosphere. The validity of the overall approach was verified by measuring bulk diffusion coefficients on a single crystal CdTe.

II. BULK AND GRAIN BOUNDARY DIFFUSION

A. Geometry

The surface morphology of physical vapor deposited films consists of densely packed hexagonal grains as shown in Fig. 1. Cross sectional analysis has shown that these grains extend continuously from the substrate to the surface. In modeling this grain configuration, we adopted a cylindrical coordinate system as depicted in Fig. 2. Each grain is divided into annular and slab elements; in cylindrical coordinates, the ith volume element, V_i, is represented as an annulus within a slab having height, Δz: $V_i=\Delta z\pi[(\rho_i+\Delta\rho)^2-\rho_i^2]$, where ρ is the radial coordinate. The volume fraction of the ith volume element, F_i, is $F_i=V_i/\Delta z\pi r^2$, where r is the grain radius. In terms of the cylindrical geometry, this becomes

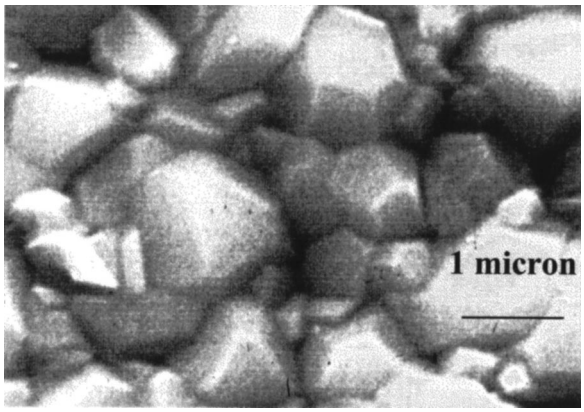

FIG. 1. SEM of as-deposited CdTe film surface.

$$F_i(\rho_i,\Delta\rho)=\frac{(\rho_i+\Delta\rho)^2-\rho_i^2}{r^2}. \tag{1}$$

B. Composition due to diffusion

For the nth slab, the composition of the ith radial element, $c_{i,n}$ is defined as the midpoint composition of the corresponding volume element: $c_{i,n}(\rho_i,z_n,t)\equiv c_g(\rho_i,z_n,t)$, where $\rho_i\equiv\Delta\rho(i+1/2)$ and $z_n\equiv\Delta z(n-1/2)$. The three-dimensional model is based on the two-dimensional solution of the diffusion equation obtained by Gilmer and Farrell for a system in which the diffusing species has a limited solubility in the film and the diffusion coefficients are independent of concentration.[6] The analytical solution found by Gilmer and Farrell applies to the following conditions: (1) isolated grain boundary, (2) constant diffusant source, (3) constant bulk and grain boundary diffusion coefficients, D and D_b, and (4) reflecting free surface. The two-dimensional solution was then transformed to three dimensions using the cylindrical symmetry.

The two-dimensional coordinate system used by Gilmer and Farrell is shown in Fig. 3. Within each grain, the concentration is assumed to obey the bulk diffusion equation:

$$D\nabla^2 c=\frac{\partial c}{\partial t},\quad 0<\rho<(r-\delta/2). \tag{2}$$

The grain boundary concentration follows a similar equation, in the lateral dimension from $(r-\delta/2)$ to $(r+\delta/2)$. The concentration within the grain boundary was assumed to have a parabolic dependence in the ρ direction. Subject to the constraints that the concentration in the film is zero at $t=0$, Eq. 2 is satisfied by functions of the form:

$$F(\rho,z,t)=\sum_{n,m=1}^{\infty} A_{nm}Y_{nm}(\rho)Z_n(z)T_{nm}(t), \tag{3}$$

where Y_{nm} and Z_n are periodic functions in the r and z directions, respectively. The assumed parabolic dependence of concentration within the grain boundary leads to the boundary condition of the form:

$$(\Delta-1)\beta_n^2-\alpha_{nm}^2=\left(\frac{2\alpha_{nm}}{\delta}\right)\tan(\alpha_{nm}r), \tag{4}$$

where $\beta_n=[\pi(2n-1)]/2h$ and $\Delta=D_b/D$, where D and D_b are the bulk and grain boundary diffusion coefficients, respectively.

The parameter α_{nm} is solved by iteration of Eq. 4. The boundary condition needed to determine the function in Eq. 3 is that which represents the physical situation at the surface of the film, at coordinate h in z. In the present case, we consider that the free surface ''reflects'' diffusant in the z direction. In the case, the incremental composition, c_g at coordinate ρ, z and time, t, is thus:

$$c_g(\rho,z,t)=c_0\left[1-\sum_{n=1}^{\infty}\sum_{m=1}^{\infty}A_{nm}Y_{nm}(\rho)Z_n(z)T_{nm}(t)\right], \tag{5}$$

where Y_{nm}, Z_n, T_{nm}, and A_{nm} are

$$Y_{nm}=\cos(\alpha_{nm}\rho), \tag{6}$$

$$Z_n=\sin(\beta_n z), \tag{7}$$

$$T_{nm}=\exp[-Dt(\alpha_{nm}^2+\beta_n^2)], \tag{8}$$

$$A_{nm}=\frac{\frac{8}{\alpha_{nm}r}\sin(\alpha_{nm}r)+\frac{4\delta}{r}\cos(\alpha_{nm}r)}{(2n-1)\pi\left(1+\frac{\sin(2\alpha_{nm}r)}{2\alpha_{nm}r}+\frac{\delta}{r}\cos^2(\alpha_{nm}r)\right)}. \tag{9}$$

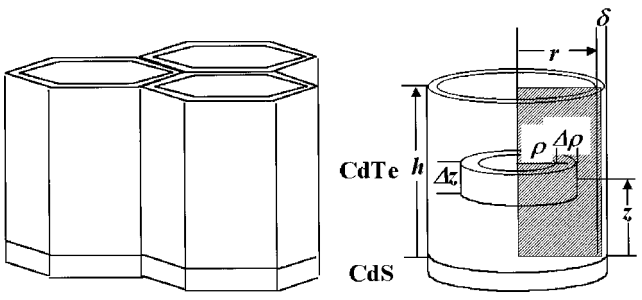

FIG. 2. Hexagonal representation of grains and cylindrical geometry used to model diffusion.

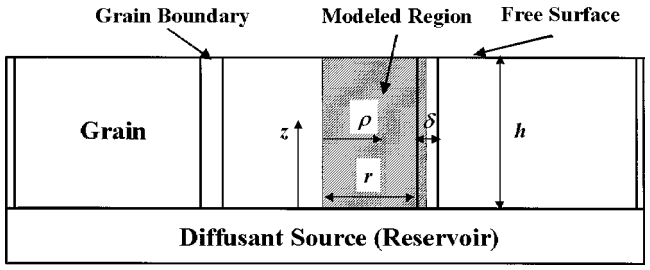

FIG. 3. Two-dimensional section through cylinder showing grain structure modeled by Gilmer and Farrell.

C. Diffraction profile from spatial composition distribution

Within each slab, the incremental composition, c_i, of a particular volume element was transformed to Bragg angle, θ_i, for a given reflection, (hkl), by the Vegard relation for the CdTe–CdS system:[7]

$$\theta_i = \arcsin\left[\frac{n\lambda\sqrt{h^2+k^2+l^2}}{2\left(6.481-\frac{c_i}{1.508}\right)}\right]. \tag{10}$$

This represents the compositional broadening of the (*hkl*) line in question. The differential power, dP_θ, diffracted from a volume element at the particular composition, or angle, in a thin homogeneous sample can be approximated in terms of the structure factor, F_{hkl} and the differential volume, dV:

$$dP_\theta \propto F_{hkl}\frac{(1+\cos^2\theta_{hkl})}{\sin\theta_{hkl}\cos\theta_{hkl}}dV. \tag{11}$$

The compositional broadening in 2θ due to formation of $CdTe_{1-x}S_x$ alloy in the temperature range considered is less than 1°. Thus, in modeling diffraction line profiles, the angular dependence of the structure factor was not considered. In this case, the differential power diffracted from a volume element is linearly proportional to its volume fraction. Within each *n*th slab, the volume fraction of the incremental composition, dP_θ, contributes to diffracted intensity or composition function, $g_n(\theta_i)$: $g_n(\theta_i)=\Sigma dP_\theta$. A line profile, $h_n(\theta_i)$, is obtained through the convolution integral of the composition function, $g_n(\theta_i)$, and the instrument function, $f_n(\theta_i)$:

$$h_n(\theta_i) = \int_{\theta_1}^{\theta_2} g_n(\theta_i) f_n(\theta_i) d\theta. \tag{12}$$

A Pearson VII function was used to simulate the diffractometer instrument intensity function:[8]

$$f = f_b + f_0\left[1+\frac{(2^{1/m}-1)x^2}{H^2}\right]^{-m}, \tag{13}$$

where x is the angular deviation from the peak centrum, H is the half width at half maximum, and m is the shape parameter. In this function, $m=1$ defines the Cauchy function while $m=\infty$ defines the Gaussian function. The (511)/(333) line profile of annealed CdTe powder with nominally 100 to 500 μm particle size yielded a diffractometer instrument function with $m=3$ and $H=0.06°$.

The intensity function for a given slab was corrected for primary and diffracted beam extinction in the overlying layers according to

$$h_n(\theta, z_n) = \exp[-2\mu_m z_n/\sin(\theta)]\int_{\theta_1}^{\theta_2} g_n(\theta) f_n(\theta) d\theta, \tag{14}$$

where μ_m is the x-ray mass absorption coefficient of the overlying medium at the measurement x-ray energy employed. In this treatment, the value of μ_m for Cu$K\alpha$ x-rays varies negligibly over the $CdTe_{1-x}S_x$ compositional range, so the value for CdTe at 8 keV was taken for $\mu_{CdTe}(8\text{ keV}) = 0.1587\,\mu\text{m}^{-1}$.

III. EXPERIMENTAL CONDITIONS AND DATA TREATMENT

A. Solubility limit determination

Accurate modeling of the $CdTe_{1-x}S_x$ alloy line profiles at different temperatures requires the alloy system equilibrium solubility limits which establish the lattice parameter range represented by diffraction line profiles. The solubility limits of the CdTe–CdS system were established by XRD determination of $CdTe_{1-x}S_x$ and $CdS_{1-y}Te_y$ alloy lattice parameters in mixed CdTe–CdS films after thermal treatment in $CdCl_2$:O_2Ar vapor from 420 °C to 625 °C. The mixed films were evaporated from CdS and CdTe powders on Corning 7059 glass, forming metastable alloys with midrange composition $\sim CdTe_{0.5}S_{0.5}$. Heat treatment of these films in $CdCl_2$:O_2:Ar vapor resulted in phase segregation into two alloy components at each side of the CdTe–CdS equilibrium miscibility gap.[9] To ensure that end-point compositions were reached at each temperature, the treatment time was extended until the measured change in alloy compositions were less than the detection limit, which, for x and y, is ~0.0001. X-ray diffraction scans were taken over the 2θ range from 20 ° to 91 °, sampling nine (*hkl*) reflections. The individual lattice parameters for each (*hkl*) were reduced to a precision lattice parameter, a_0, by extrapolation on a plot of a_0 versus Nelson–Riley–Sinclair–Taylor function[10] CdS weight fraction, x, in zincblende $CdTe_{1-x}S_x$ and CdTe weight fraction, y, in wurtzite $CdS_{1-y}Te_y$ were calculated from the precision lattice parameter using $x=1.508(6.481-a_0)$ and $y=1.508(a_0-4.136)$.

B. Sample preparation

Thin-film CdTe/CdS structures were fabricated in substrate configuration on Corning 7059 glass coated with a 1 μm thick film of molybdenum and a 100 nm thick film of CuTe. CdTe films 4.5 μm thick were deposited by thermal evaporation at 250 °C onto the substrate at 3 nm/s from 99.999% purity CdTe powder. Undoped (111)-oriented CdTe single crystal wafers obtained from Keystone Crystal Corporation were also used as substrates, for Auger electron depth profile measurements of sulfur concentration after treatment. In all cases, CdS films from 200 to 220 nm thick were deposited at 220 °C by thermal evaporation at 0.3 nm/s from 99.999% purity CdS powder.

C. Vapor treatment

All CdTe/CdS structures were vapor treated in $CdCl_2$:O_2:Ar in a 6 cm diameter tubular reactor configured to deliver $CdCl_2$ vapor at a fixed concentration for different reaction temperatures, from 380 °C to 480 °C for 0.5 to 40 min.[11] Oxygen concentration was maintained at a partial pressure of ~130 Torr by adjusting volume flow rate with argon balance, maintaining a constant total flow of 1.0 1/m through the reaction zone. $CdCl_2$ vapor was generated from a sintered powder source contained in a graphite susceptor within 1 mm of the CdTe surface. $CdCl_2$ partial pressure was maintained at ~10 mTorr by controlling the $CdCl_2$ susceptor temperature at ~415 °C. At a total pressure of 1 atm. trans-

TABLE I. Measured solubility limits of the CdTe–CdS system.

Temperature (°C)	x in $CdTe_{1-x}S_x$	y in $CdS_{1-y}Te_y$
625	0.140	0.10
525	0.095	0.07
415	0.058	0.03

port of $CdCl_2$ vapor to the sample surface is diffusion limited, with a time constant of ~0.2 s. which is sufficiently small with respect to treatment time to allow equilibrium to be maintained with respect to $CdCl_2$ vapor.[11]

Prior to each treatment, the assembly containing the $CdCl_2$ source and CdTe/CdS structures was baked in vacuum at 250 °C for 15 min. to dehydrate the $CdCl_2$ and the surface of the CdTe. From this temperature, the treatment temperature at the substrate surface was attained in ~30 s. Cooldown rates of ~200 °C per minute were achieved by shutting off power to the heating lamps.

D. Sample analysis

The film surfaces were examined by scanning electron microscopy (SEM) using an Amray 1810 T microscope at 30 kV and by atomic force microscopy using a Digital Instruments Dimension 3100 microscope in tapping mode. Grain radii, defined as the mean lateral half dimension of clearly delineated grains, were determined from micrographs taken at three different positions on each film sample. Grain radii varied and were categorized in 0.5μm intervals from 0 to 2 μm, sampling >300 grains. This data was used to generate a frequency distribution for each grain size interval. Grain boundary widths were estimated from cross sectional transmission electron micrographs of CdTe/CdS thin-film structures deposited on Si single crystals.

XRD scans of the films were performed using a Philips/Norelco Bragg–Brentano focusing diffractometer with Cu$K\alpha$ radiation at 35 kV. Line profiles of the $CdTe_{1-x}S_x$(511)/(333) reflection were acquired by step scanning in 0.02° intervals from 76.0 to 77.0° in 2θ. An instrument function for pure CdTe was obtained using an annealed CdTe powder sample and yielded a half width at half maximum, H, of 0.06°. XRD data was smoothed, and the $K\alpha_2$ component was stripped using the Rachinger correction.[12] For quantitative comparison purposes, the background intensity was removed, and the resulting profiles were normalized to the area of the untreated (511)/(333) reflection.

Auger electron depth profiles of sulfur concentration were obtained from single crystal substrates at different temperatures to provide independent values of bulk diffusion coefficient for comparison with values obtained by the modeling of XRD line profiles. The diffusion coefficient was calculated from the data using the solution for diffusion into an infinite medium with a constant surface concentration.[13]

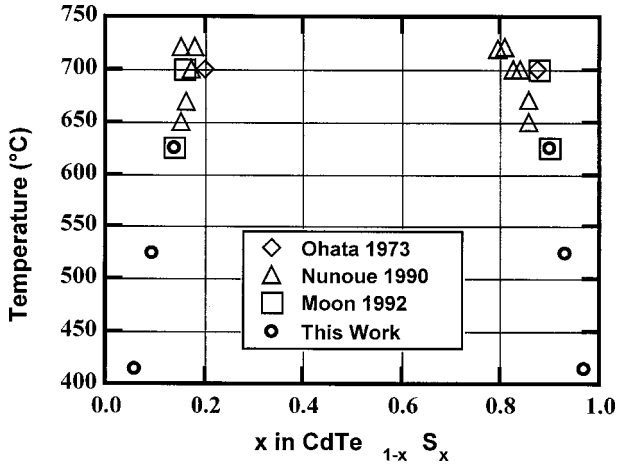

FIG. 4. T-x phase diagram for CdTe–CdS alloy system, comparing solubility limits in mixed CdTe–CdS films treated in $CdCl_2$:O_2:Ar vapor at 415 °C to 625 °C (this work) to solubility limits determined by Moon *et al.*,[14] Nunoue *et al.*, and Ohata, *et al.*[15]

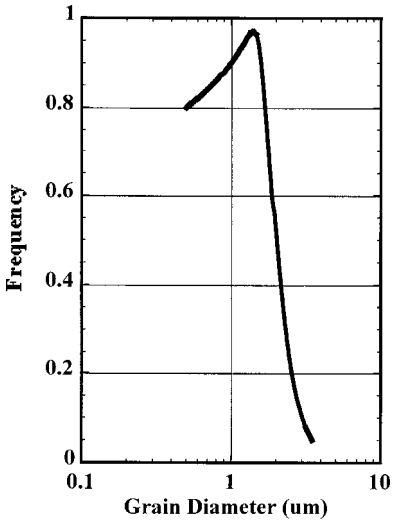

FIG. 5. Grain size distribution to model diffusion of CdS into CdTe thin films.

IV. RESULTS

A. Solubility limit determination

The measured solubility limits at three treatment temperatures are listed in Table I. The values obtained at 625 °C coincide with those measured by Moon *et al.*[14] for the system without $CdCl_2$:O_2:Ar, indicating that these vapor species do not affect the end-point equilibrium compositions. Rather, $CdCl_2$ and O_2 vapor enhance the kinetic processes responsible for diffusion. The provisional CdTe–CdS phase diagram, extended down to 415 °C, is shown in Fig. 4, incorporating the high temperature data of other groups.[14,15] For carrying out modeling at temperatures below 415 °C, solubility limit values were estimated by extrapolation of the phase boundary on Fig. 4, using the empirical fit

$$x = -0.0149 + (1.207\times10^{-4})T + (3.940\times10^{-8})T^2 + (2.393\times10^{-10})T^3, \quad (15)$$

for T in Celsius.

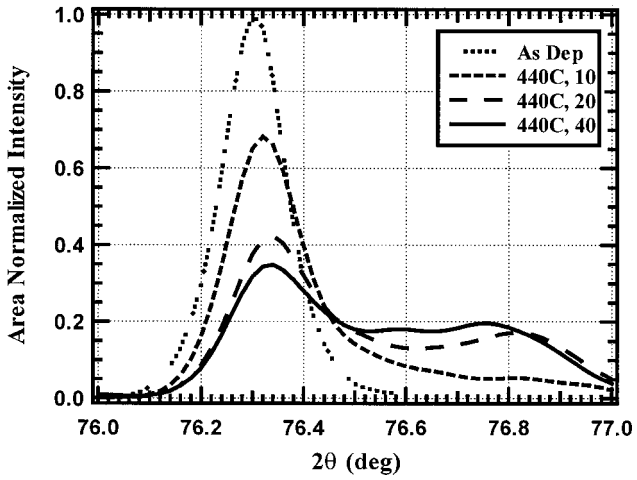

FIG. 6. Measured XRD (511)/(333) line profiles for as-deposited and time progressively heat treated CdTe/CdS thin film couples. Heat treatment was carried out in $CdCl_2$:O_2:Ar vapor at 440 °C for the times shown.

B. Grain size distribution

The grain size distribution used to model line profiles is shown in Fig. 5. This measured distribution was converted to the volume fractional contribution for 10 grain size intervals. For each treatment time, the diffusion model was calculated for the corresponding volume fraction of each interval. These contributions to the compositional profiles were summed to produce the composite result. The functional form of the grain size distribution differs from a log-normal distribution for the mean grain size of this grain population. From volume fractional considerations, the peak in the grain size distribution does not represent the actual contribution of each grain size to diffracted intensity, which can lead to skewing of the final compositional profile. For the model, overestimating the grain radius, r, reduces the grain boundary contribution and skews the compositional result toward lower sulfur concentration. Conversely, underestimating grain radius amplifies the grain boundary diffusion contribution, skewing the compositional result toward high concentration.

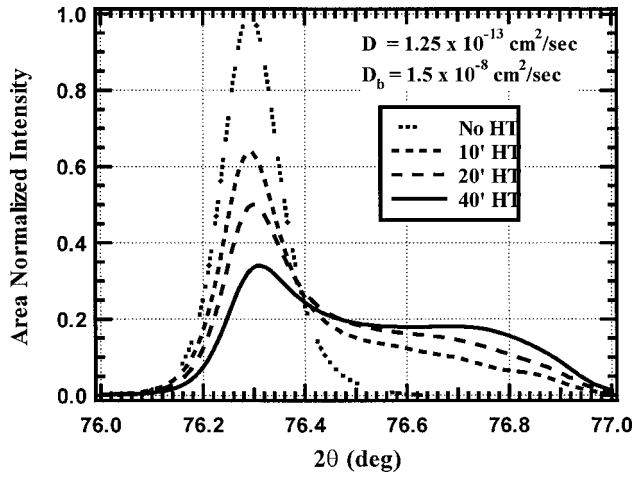

FIG. 7. Modeled XRD (511)/(333) line profiles for as-deposited and time progressively heat treated CdTe/CdS thin film couples using the bulk and grain boundary diffusion coefficients and times shown.

TABLE II. Bulk and grain boundary diffusion coefficients used to model the measured XRD line profiles at different treatment temperatures.

Temperature (°C)	D (cm^2/s)	D_b (cm^2/s)	Δ
400	8.00×10^{-15}	3.00×10^{-9}	3.7×10^{5}
440	1.25×10^{-13}	1.50×10^{-8}	1.2×10^{5}
475	1.80×10^{-12}	8.00×10^{-8}	4.4×10^{4}

C. Measured and modeled XRD line profiles

The measured diffraction line profiles for films treated before treatment and for 10, 20, and 40 min treatment at 440 °C are shown in Fig. 6. The profile evolution from 10 to 40 min is characterized by continuous transformation of pure CdTe into $CdTe_{1-x}S_x$ alloy. Within a small margin, the four profiles exhibited the same integrated area, which is consistent with the observation that the films had the same orientation, regardless of treatment.

Modeled diffraction line profiles for the times of Fig. 6 are shown in Fig. 7. The following input parameters were used to generate the line profiles of Fig. 7: $D=1.25\times10^{-13}\,cm^2/s$; $D_b=1.50\times10^{-8}\,cm^2/s$ ($\Delta=1.2\times10^5$); $\delta=2$ nm; and 10 values of grain radii with frequency of each grain size taken from Fig. 5. Only a narrow range of diffusion coefficients, $\pm20\%$, allowed the observed time-progressive profiles to be represented by the modeled time-progressive profiles. The grain boundary distribution was critical to matching the line profiles, especially with respect to the bimodal shape of the 20 min profile.

D. Activation energy of diffusion

Measured diffraction line profiles were also modeled for results obtained at different treatment temperatures and fixed $CdCl_2$:O_2:Ar vapor concentration using the bulk and grain boundary diffusion coefficients shown in Table II. Comparative values for the bulk diffusion coefficients over this temperature range were obtained by analysis of the Auger electron depth profiles of sulfur distribution in single crystals and are listed in Table III. The combined bulk diffusion coefficient data is shown in Fig. 8, giving an activation energy of 2.8 eV for bulk diffusion of CdS into CdTe. This activation energy is the same as has been reported for the self-diffusion of Cd in CdTe attributed to formation of singly ionized Cd interstitials.[16] For the films, the grain boundary diffusion coefficients obtained at the three temperatures yield an activation energy of 2.0 eV (Fig. 9).

TABLE III. Bulk diffusion coefficient obtained from Auger depth profiles of sulfur distribution in CdTe single crystals after treatment.

Temperature (°C)	D (cm^2/s)
390	5.0×10^{-15}
420	3.0×10^{-14}
450	1.5×10^{-13}

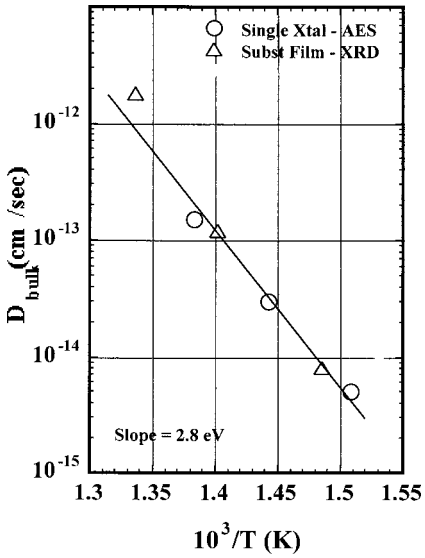

FIG. 8. Arrhenius plot of bulk diffusion coefficients vs inverse of treatment temperature for values obtained by modeling XRD line profiles of thin film CdTe/CdS and from Auger electron depth profiling of sulfur distribution in CdTe single crystal.

The arrays used to generate the compositional distribution allow a two-dimensional isocomposition map to be easily constructed. Figure 10 shows a two-dimensional isocompositional cross section plot through grains of two different radii for a 40 min solution with diffusion coefficients $D = 1.25\times10^{-13}\,\mathrm{cm}^2/\mathrm{s}$ and $D_b = 1.50\times10^{-8}\,\mathrm{cm}^2/\mathrm{s}$. In this example, the small grain no longer contains pure CdTe, while the larger grain is composed of alloys through the entire compositional range from CdTe to $CdTe_{0.94}S_{0.06}$, corresponding to a band gap variation of 1.51 to 1.45 eV.[7]

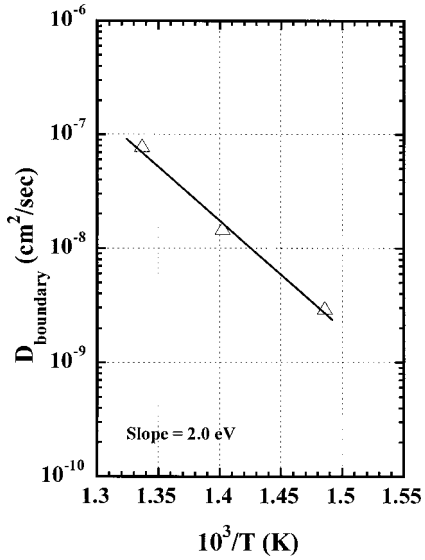

FIG. 9. Arrhenius plot of grain boundary diffusion coefficients vs inverse of treatment temperature obtained by modeling XRD line profiles of thin film CdTe/CdS structures.

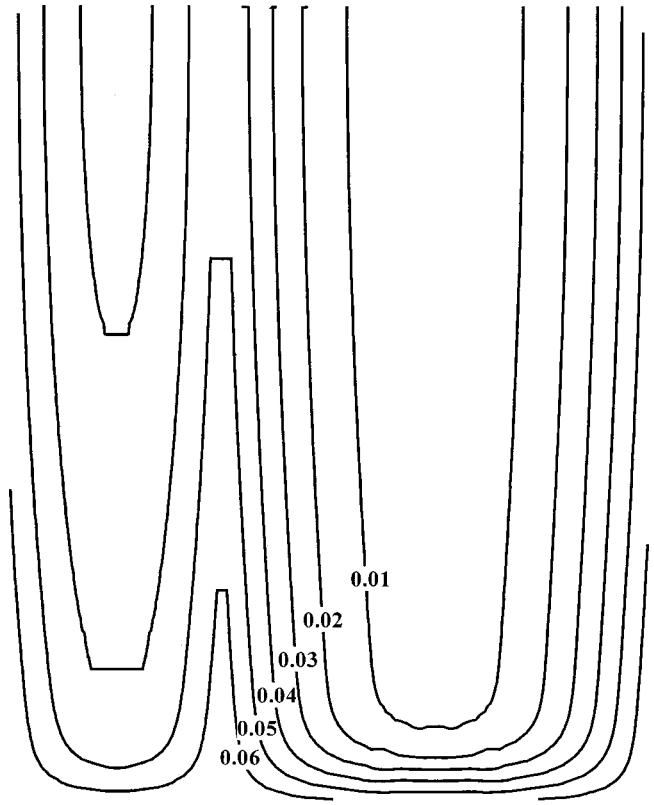

FIG. 10. Two-dimensional isocompositional contour plot of sulfur distribution after diffusion for 40 min with $D = 1.25\times10^{-13}\,\mathrm{cm}^2/\mathrm{s}$ and $D_b = 1.5\times10^{-8}\,\mathrm{cm}_2/\mathrm{s}$ for grains of a 4.5 μm thick film with grain radii of 0.25 and 0.5 μm. Isocontours are incremented by x in $CdTe_{1-x}S_x$ in steps of 0.01.

V. CONCLUSIONS

The diffusion of CdS into CdTe polycrystalline thin films that occurs during heat treatment in $CdCl_2$:O_2:Ar vapor can be represented by a simple three-dimensional model that accounts for bulk and grain boundary diffusion and grain size distribution. Regressing modeled XRD line profiles to measured profiles for thin-film samples time progressively treated yielded values for the bulk and grain boundary diffusion coefficients and their activation energies. Uniqueness of the solutions are ensured by fitting time progressive cases. The bulk diffusion coefficients were verified by Auger analysis of single crystal CdTe samples. This method can be used to investigate the effects of treatment ambient composition on bulk and grain boundary diffusion, leading to an atomistic description of the diffusion process. In thin-film electronic devices such as solar cells, variations in composition can be determined to aid analysis of device operation.

ACKNOWLEDGMENTS

The authors wish to thank Shannon Fields, Kevin Hart, and Herbert Wardell for sample preparation, D. Garth Jensen and Gregory M. Hanket for contributing to the determination of solubility limits, Erten Eser and James E. Phillips for valuable discussions, and Elaine Koronik for help in preparing the manuscript. This work was supported by the United

States Department of Energy through a grant from the National Renewable Energy Laboratory, Contract Number ZAK-8-17619-33.

[1] J. Britt and C. Ferekides, Appl. Phys. Lett. **62**, 2851 (1993).
[2] B. E. McCandless and R. W. Birkmire, Proceedings of the 26th IEEE Photovoltaic Specialists Conference, 1997 p. 307.
[3] B. E. McCandless, I. Youm, and R. W. Birkmire, Prog. Photovoltaics **7**, 21 (1999).
[4] M. K. Herndon, A. Gupta, V. Kaydanov, and R. T. Collins, Appl. Phys. Lett. **75**, 3503 (1999).
[5] D. W. Lane, K. D. Rogers, J. D. Painter, D. A. Wood, and M. E. Ozsan, Thin Solid Films **361**, 8 (2000).
[6] G. Gilmer and H. Farrell, J. Appl. Phys. **47**, 4373 (1976).
[7] B. E. McCandless, L. V. Moulton, and R. W. Birkmire, Prog. Photovoltaics **5**, 249 (1997).
[8] R. A. Young and D. B. Wiles, J. Appl. Crystallogr. **15**, 430 (1982).
[9] D. G. Jensen, B. E. McCandless, and R. W. Birkmire, Proceedings of MRS Symposium, Vol. 426, San Francisco, CA, 1996, pp. 325–330.
[10] C. Barrett and T. B. Massalski, *Structure of Metals*, 3rd ed. (Pergammon, Oxford, 1980) p. 144.
[11] B. E. McCandless, H. Hichri, G. Hanket, and R. W. Birkmire, Proceedings of the 25th IEEE Photovoltaic Specialist Conference (1996) 781.
[12] B. E. Warren, *X-ray Diffraction* (Addison–Wesley, Reading, MA, 1969).
[13] P. G. Shewmon, *Diffusion in Solids* (McGraw–Hill, New York, 1963) p. 14.
[14] D. G. Moon and H. B. Im, Powder Metall. **35**, 53 (1992).
[15] K. Ohata, J. Saraie, and T. Tanaka, Jpn. J. Appl. Phys. **12**, 1198 (1976).
[16] J. H. Crawford and L. M. Slifkin, *Point Defects in Solids* (Plenum, New York, 1975), pp. 227–256.